EAA Benchmark for an axial fan

Manfred Kaltenbacher, Stefan Schoder

EAA BENCHMARK FOR AN AXIAL FAN

Manfred Kaltenbacher
Mechanics and Mechatronics
TU Wien, Austria
Fundamentals and Theory in Electrical Engineering
TU Graz, Austria
manfred.kaltenbacher@tugraz.at

Stefan Schoder
Fundamentals and Theory in Electrical Engineering
TU Graz, Austria
stefan.schoder@tugraz.at

ABSTRACT

We present detailed numerical results of the EAA benchmark case of an axial fan. Thereby, we aim to present the whole aeroacoustic simulation process for a successful computation of the flow and acoustic signature of an axial fan: (1) Meshing approach for the CFD simulation; (2) Turbulence modeling; (3) CFD convergence study; (4) Evaluation of the most significant flow results for a subsequent acoustic simulation; (5) Computational domain and meshing for the simulation of the acoustic field; (6) Acoustic source term evaluation, possible truncation and interpolation from the CFD to the acoustic grid; (7) Acoustic field computation and evaluation of its most relevant physical quantities.

1. INTRODUCTION

Solutions to the partial differential equations that describe acoustic problems can be found by analytical, numerical and experimental techniques. Within arbitrary domains and for arbitrary initial and boundary conditions, all solution techniques require certain assumptions and simplifications. Over the years many researchers in the field of computational acoustics have therefore expressed the need and wish to have available common benchmark cases. Therefore, we have started an initiative to setup a common web-based database, where cases and results can be submitted by all researchers and are openly available [1]. This contribution is intended to provide main information about the EAA benchmark case of an axial fan [2].

2. AXIAL FAN: SETUP

The investigated axial fan is displayed in 1. The fan had nine fan blades and a tip diameter of $495\,\mathrm{mm}$. It was installed inside a duct with a diameter of $500\,\mathrm{mm}$, hence the tip gap was $2.5\,\mathrm{mm}$. The fan is embedded in a sound hard tube and all measurements are performed in a standardized inlet test chamber according to ISO 5801. The test chamber was built as an anechoic chamber with absorbing walls, ceiling, and floor, to enable aeroacoustic measurements. The rotational speed of the fan is about $1500\,\mathrm{rpm}$, which results in a maximum tip speed of $38.89\,\mathrm{m/s}$. The fan was installed in a short duct with a bellmouth on the in- and outlet to resemble a realistic test setup. The fan

(a) Axial fan.

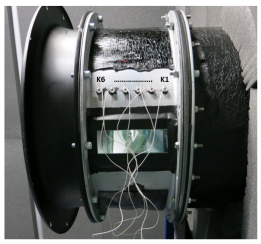

(b) Pressure sensors K1 to K6.

Figure 1: Axial fan and position of the pressure sensors.

was driven by a motor inside the duct. Torque and rotational speed were measured with a precision torque meter. To ensure that torque measurements are not compromised by frictional torque of the bearings, an offset measurement was performed with the fan being removed. For all details, we refer to [3].

3. CFD COMPUTATIONS

For the numerical computation of the flow field, OpenFOAM Toolbox version 2.3.0 has been used to solve the incompressible Navier-Stokes equations based on the finite-volume method and the arbitrary mesh interface (AMI). The AMI allows simulation across disconnected, but adjacent mesh domains, which are especially required for rotating geometries. The computational domain is displayed in Fig. 2a including the axial fan inside the pipe, the inlet chamber, and the outlet region. The flow solution is

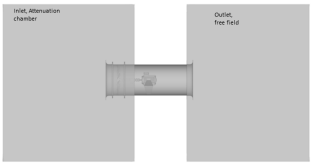

(a) Computational domain for flow computation.

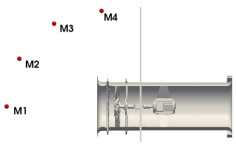

(b) Microphone positions.

Figure 2: Computational domain for flow computation and position of the microphones.

computed using an adapted version of the pimpleDyMFoam solver, which can handle dynamic meshes, with a time step size of $\Delta t = 10\,\mu\mathrm{s}$. For the CFD computation,

a hexahedron-dominant finite volume mesh consisting of 29.8 million cells was generated with the automatic mesh generator HEXPRESSTM / Hybrid from Numeca, as displayed in Fig. 3a. The transient simulation was carried out by using a detached-eddy simulation based on the Spalart-Allmaras turbulence model to accurately resolve the complex flow field. The applied finite-volume scheme is second order in space and time, and the convective term has been discretized by a bounded central upwind scheme. All calculations were performed on the Vienna Scientific Cluster VSC2 with 256 cores. In total, the CFD computation

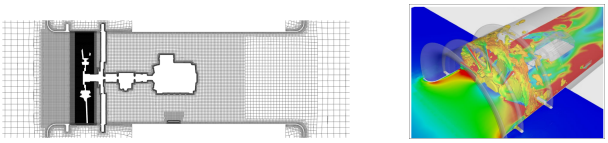

(a) Computational grid. (b) Flow structure.

Figure 3: Cross section through the computational mesh for CFD and flow structure for a characteristic time step.

has been performed for 10 revolutions. After about 6 revolutions, the flow field achieved steady-state and we used the CFD data of the remaining 4 revolutions for acoustic source and wave propagation computation. Figure 3b displays the flow structure for a characteristic time step.

To validate the flow computation, wall pressure fluctuations [1] were measured with 6 differential miniature pressure transducers XCS-093-1psi D (Kulite Semiconductor Products) with a diameter of 2.5 mm (see Fig. 1b). The differential pressure was measured concerning the pressure inside the test chamber. The sensors were flush mounted and equally spaced along a line on the duct. Exemplary, we show the spectral density of the instationary pressure in Fig. 4 at position K2 and K4 (for position see Fig. 1b). Here, we want to note that especially a good comparison between measured and simulated pressure spectra is of high relevance since the instationary pressure is a key physical quantity within aeroacoustic computations.

4. SOURCE TERM INTERPOLLATION AND ACOUSTIC FIELD COMPUTATION

In accordance to the flow computation, the rotating domain is embedded into a quiescent propagation region for performing the acoustic simulations (see Fig. 5) [4, 5]. Furthermore, we add at the inflow and outflow boundaries of the CFD domain two additional regions, on which we apply a PML to effectively approximate acoustic free field conditions [6]. To resolve accurately the rotor geometry, we use tetrahedron elements as displayed in Fig. 5b. As soon as we approach the inlet as well as the outlet, we use hexahedron elements and combine the meshes by our Nitsche-type mortaring approach. Here, we want to note that the discretization of the rotating and station-

[1] It is especially important to validate relevant flow quantities that are connected to the aeroacoustic source term. The space-time and time-harmonic distribution should be validated. In this case, the main source term is connected to the incompressible pressure.

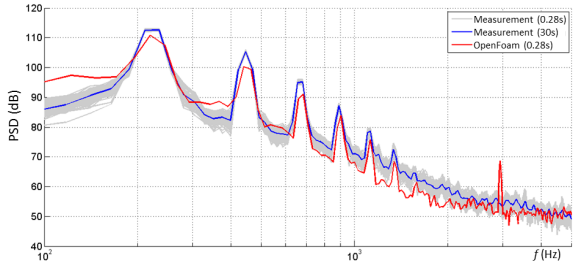

(a) Position 2

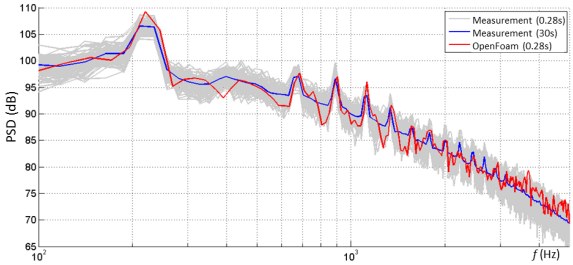

(b) Position 4

Figure 4: Spectral density (relative to 20μPa) of the measured instationary pressures at position K2 and K4.

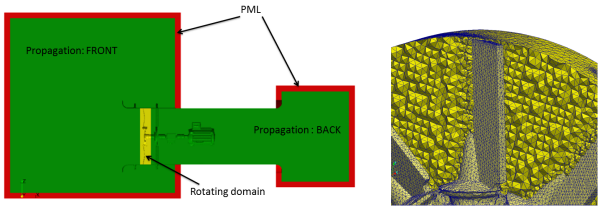

(a) Computational setup (b) Detail of mesh

Figure 5: Computational domain for the acoustic calculation and detail of acoustic mesh near the rotor.

ary domain has been performed individually by the preprocessor, which strongly reduces the effort of the mesh generator and improves the mesh quality. Finally, the computational mesh resulted in approximately 2 million cells, which is by a factor of 15 smaller than the flow grid. Here, we want to emphasize that the acoustic grid has been adjusted toward high quality for solving the wave equation. This means that the cells should have less deformation (no stretched cells as used in flow computation to resolve boundary layers) and have a similar size all over the computational domain to accurately resolve the wave propagation. Thereby, the spatial resolution of the mesh has been chosen to resolve acoustic waves up to 5 kHz (about ten finite elements with linear basis functions per wavelength), which was the main frequency range of interest. The used time-stepping scheme with controlled dispersion (Hilber-Hughes-Taylor) numerically damps waves of higher frequency to avoid numerical artifacts. Therefore, the computed acoustic spectra will strongly decrease above 5 kHz (see Figs. 6a and 6b). The mesh convergence has been studied by placing artificial sources on the rotor blades. We perform the computation of the acoustic sources on the flow grid and then apply the cut-volume-

cell approach to interpolate to the acoustic grid [7]. The acoustic source computation, its interpolation to the acoustic grid and the computation of the acoustic field has been performed by the in-house research software CFS++ (Coupled Field Simulation) [8].

The sound field was measured with four 1/2 inch free-field microphones, type 4189-L-001 (Brüel & Kjaer) arranged in a quarter-circle with a radius of 1 m around the inlet bellmouth in a horizontal plane at the same height as the rotational axis, see Fig. 2b. Thereby, the measurements were made synchronized with the wall pressure fluctuations. Accordingly, measurement time was 30 s with a sampling frequency of 48 kHz. Figures 6 display the computed power spectral density of the acoustic pressure at the two microphone positions (for location see Fig. 2b) and compares it to the measured one. Thereby, we display the smoothed measured spectra obtained from the 30 s recorded acoustic pressure signals as well as the individual spectra by just using measured data of 0.1 s (in gray). The computed spectra based on our numerical simulation is calculated out of a real-time simulation of 0.06 s. For further

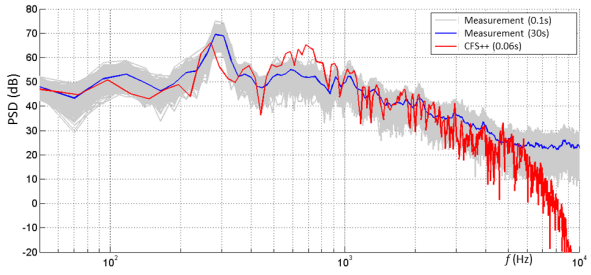

(a) Position M1

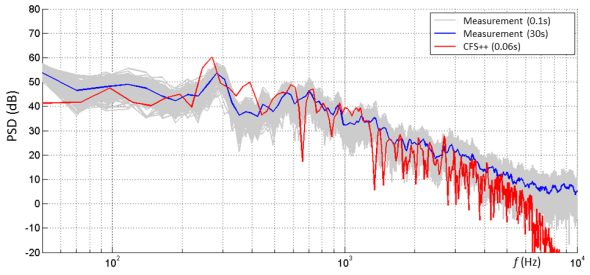

(b) Position M4

Figure 6: Spectral density (relative to 20μPa) of the measured microphone signals at position M1 and M4.

details, we refer to [9].

5. CONCLUSION

We have presented our numerical approach and obtaind results for the EAA benchmark case of an axial fan [2]. We hope to attrack many scientists to also perform numerical computations for this EAA benchmark case and present their results on upcoming conferences as well as publications in scientific journals.

6. REFERENCES

[1] M. Hornikx, M. Kaltenbacher, and S. Marburg, "A platform for benchmark cases in computational acoustics," *Acta Acustica united with Acustica*, vol. 101, no. 4, pp. 811–820, 2015. https://doi.org/10.3813/AAA.918875.

[2] "Acoustics involving heterogeneous and moving fluids: Axial fan." https://eaa-bench.mec.tuwien.ac.at/benchmarks/acoustics_involving_heterogeneous_and_moving_fluids/axial_fan/. Accessed: 2020-10-30.

[3] F. Zenger, C. Junger, M. Kaltenbacher, and S. Becker, "A benchmark case for aerodynamics and aeroacoustics of a low pressure axial fan," in *SAE Technical Paper*, SAE International, 06 2016.

[4] M. Kaltenbacher, A. Hüppe, A. Reppenhagen, F. Zenger, and S. Becker, "Computational aeroacoustics for rotating systems with application to an axial fan," *AIAA journal*, pp. 3831–3838, 2017. https://doi.org/10.2514/1.J055931.

[5] M. Kaltenbacher, *Computational Acoustics*. CISM International Centre for Mechanical Sciences, Springer International Publishing, 2018.

[6] B. Kaltenbacher, M. Kaltenbacher, and I. Sim, "A modified and stable version of a perfectly matched layer technique for the 3-d second order wave equation in time domain with an application to aeroacoustics," *Journal of Computational Physics*, vol. 235, no. 0, pp. 407 – 422, 2013. http://www.sciencedirect.com/science/article/pii/S0021999112006055.

[7] S. Schoder, K. Roppert, M. Weitz, C. Junger, and M. Kaltenbacher, "Aeroacoustic source term computation based on radial basis functions," *International Journal for Numerical Methods in Engineering*, vol. 121, no. 9, pp. 2051–2067, 2020. https://onlinelibrary.wiley.com/doi/abs/10.1002/nme.6298.

[8] M. Kaltenbacher, *Numerical Simulation of Mechatronic Sensors and Actuators – Finite Elements for Computational Multiphysics*. Berlin: Springer, 3. ed., 2015.

[9] Schoder, Stefan, Junger, Clemens, and Kaltenbacher, Manfred, "Computational aeroacoustics of the eaa benchmark case of an axial fan," *Acta Acustica*, vol. 4, no. 5, p. 22, 2020. https://doi.org/10.1051/aacus/2020021.